

Effect of a Small Amount of Cr and Mo on Aqueous CO₂ Corrosion of Low-Alloyed Steel and Formation of Protective FeCO₃ in Near-Saturation Conditions

Keiichi Kondo,^{***} Yoon-Seok Choi,^{†,*} and Srdjan Nešić^{*}

The effect of a small amount (1 wt%) of Cr or Mo on aqueous CO₂ corrosion of low-alloyed steel and the formation of protective FeCO₃ corrosion product layers was investigated under controlled water chemistry conditions, where the bulk saturation value of FeCO₃ was maintained at near-saturated condition. Changes in CO₂ corrosion rate with exposure time were monitored by linear polarization resistence measurements. The surface morphology and the composition of the corrosion product layers were analyzed by scanning electron microscopy, energy dispersive x-ray spectroscopy, x-ray diffraction, and transmission electron microscopy. Results showed that the emergence of a continuous Fe₃C layer created favorable conditions at the surface of nonalloyed steel (containing no Cr and Mo) for semiprotective FeCO₃ to form even though the bulk saturation value of FeCO₃ was maintained at near-saturated condition. However, semiprotective FeCO₃ was not observed on the surface of 1% Cr steel and 1% Mo steel, but rather discontinuous and porous corrosion product layer was formed. Due to the hydrolysis reactions of Cr³⁺ and Mo³⁺, and the discontinuous structure of the corrosion product layers, the surface conditions for 1% Cr steel and 1% Mo steel were not favorable for the formation of FeCO₃ under the experimental conditions of this study.

KEY WORDS: alloy elements, carbon steel, CO₂ corrosion, iron carbonate

INTRODUCTION

One area of critical importance in CO₂ corrosion of mild and low alloy steels is the precipitation of protective iron carbonate (FeCO₃) corrosion product layers on the steel surface. The layer forms on the corroding surface blocking the underlying steel from further dissolution and acting as a diffusion barrier, thereby reducing the corrosion rate. Solid FeCO₃ forms when the concentrations of Fe²⁺ and CO₃²⁻ exceed the solubility limit according to the following reaction:¹⁻²



The precipitation rate of FeCO₃ depends on its saturation level, which is defined by:

$$S_{\text{FeCO}_3} = \frac{c_{\text{Fe}^{2+}} \cdot c_{\text{CO}_3^{2-}}}{K_{\text{sp}}} \quad (2)$$

where $c_{\text{Fe}^{2+}}$ is the ferrous ion concentration in mol/L, $c_{\text{CO}_3^{2-}}$ is the carbonate ion concentration in mol/L, and the solubility product of FeCO₃ (K_{sp}) is calculated using an equation proposed by Sun, et al.:³

$$\log K_{\text{sp}} = -59.3498 - 0.041377T_{\text{K}} - \frac{2.1963}{T_{\text{K}}} + 24.5724 \log T_{\text{K}} + 2.518I^{0.5} - 0.657I \quad (3)$$

where T_{K} is the temperature in Kelvin, and I is the ionic strength. FeCO₃ will not form, and any existing FeCO₃ will dissolve if the local saturation level is less than 1. The properties of FeCO₃ are affected by numerous parameters such as water chemistry, temperature, fluid flow, steel composition, and microstructure.

According to previous studies, adding small amounts of Cr (0.5% to 3%) could enhance the corrosion resistance of low alloy steels in aqueous CO₂ environments.⁴⁻¹² More specifically, it was suggested that the addition of Cr contributes to the formation of Cr(OH)₃ within FeCO₃, which causes the corrosion product layers to be more protective. Furthermore, it has been claimed that the presence of Cr³⁺ in the solution has a beneficial effect on the precipitation and growth rate of FeCO₃. This suggests that the effect of adding a small amount of Cr to the steel can be beneficial when the conditions are favorable for the formation of FeCO₃ corrosion product layers. In addition, there has been an attempt to add small amounts of Mo in combination with Cr in order to improve the corrosion resistance of low alloy steels.¹³ It reportedly contributes to the formation of a more dense and adherent corrosion product layer, when compared to the nonalloyed steel. However, the individual effect of Mo on the formation of protective FeCO₃ is not clear and has not been well addressed in the literature.

Although there are numerous studies about the effect of small amounts of Cr and Mo on the corrosion behavior of low

Submitted for publication: March 30, 2022. Revised and accepted: November 4, 2022. Preprint available online: November 4, 2022, <https://doi.org/10.5006/4100>.

[†] Corresponding author. E-mail: choiy@ohio.edu.

^{*} Institute for Corrosion and Multiphase Technology, Department of Chemical & Biomolecular Engineering, Ohio University, Athens, Ohio 45701.

^{**} Current affiliation: NIPPON STEEL CORPORATION, 1850, Minato, Wakayama, 640-8555, Japan.

Table 1. Chemical Compositions of High Strength Steels Used in the Present Study (wt%, balance Fe)

Steel Type	C	Si	Mn	P	S	Cr	Mo
Nonalloyed steel	0.24	0.34	0.98	0.011	0.0008	–	–
1% Cr steel	0.24	0.35	0.98	0.011	0.0008	1.01	–
1% Mo steel	0.22	0.34	1.00	0.011	0.0007	–	0.99

alloy steel in CO₂ environments, not many studies have properly accounted for the effect of water chemistry. As described above, the addition of Cr or Mo could affect the surface conditions of the steel, especially for the formation of protective FeCO₃. Uncontrolled water chemistry can cause variations in Fe²⁺ concentration, pH drift, and changes in CO₂ speciation during the experiment. This could compromise the investigation of the effect of those alloying elements on the formation of protective corrosion product layers on the steel surface.¹⁴ Thus, in the present study, the individual effects of Cr and Mo on the formation of FeCO₃ were evaluated in CO₂ environments where the water chemistry of the system was tightly controlled over the course of the experiments.

EXPERIMENTAL PROCEDURES

2.1 | Materials

Three low alloy steels with different chemical compositions were prepared as “nonalloyed steel” containing no Cr and Mo, “1% Cr steel,” and “1% Mo steel.” Chemical compositions of the three low alloy steels were shown in Table 1. The steels were fabricated using a vacuum arc-melting furnace and cast into 180 kg ingots. The ingots were hot rolled into plates with 15 mm thickness, and the plates were then cooled in the air at room temperature. The plates were reheated to conduct double quenched & tempered (Q&T) heat treatment by a laboratory furnace. The quenched steel plates were tempered at several temperatures to control the yield strength. Holding time was approximately 60 min at each tempering temperature (460°C for nonalloyed steel, 525°C for 1% Cr steel, and 650°C for 1% Mo steel). Figure 1 showed the microstructure of steels with different alloying elements. The basic microstructure of all steel specimens was tempered martensite. It was confirmed by TEM observation that carbides are dispersed in the matrix of each steel as particles with various sizes of around approximately 100 nm.

Specimens were machined into a rectangular shape (1.27 cm × 1.27 cm × 0.254 cm) for both electrochemical tests and surface analysis. The specimens were sequentially ground with 180, 400, and then 600 grit silicon carbide (SiC) paper, cleaned with isopropyl alcohol in an ultrasonic bath, and dried. To expose only one side of the specimen, the other side was coated either with xylan (specimen used for surface analysis) or mounted in epoxy (specimen used for electrochemical measurements).

2.2 | Glass Cell Setup with Controlled Water Chemistry

Figure 2 showed the schematic of the experimental setup. Corrosion tests were performed in a 3.8-L glass cell. The electrochemical setup consists of a three-electrode corrosion cell (working electrode [WE]: rectangular steel specimen, counter electrode [CE]: a platinum-coated titanium mesh, reference electrode [RE]: a saturated silver/silver chloride [Ag/AgCl] electrode). The system included a hot plate equipped with a temperature controller, pH electrode, sparge tube connected to the CO₂ gas inlet, and a water condenser at the gas outlet. The stationary specimen holders with seals made it easier to retrieve specimens from the test solution without oxygen contamination during the experiment used for surface analysis (Figure 2[b]). Seven specimens (one specimen for electrochemical measurement and six specimens for surface analysis), identical in size, were placed in specimen holders at the same radial distance (7 cm) from the center of the glass cell. A flow was created by a Rushton-type impeller with 20 rpm, which is equivalent to 0.3 m/s in a 0.1 m inner diameter (ID) pipe.¹⁵ The solution volume to specimen area ratio was 3.36 mL/mm². All corrosion specimens (those for electrochemical measurements and surface analysis) experienced identical flow characteristics—mass transfer rate and wall shear stress. In order to keep the amount of Fe²⁺, which directly affects the saturation level of FeCO₃, at a desired concentration during the testing period,

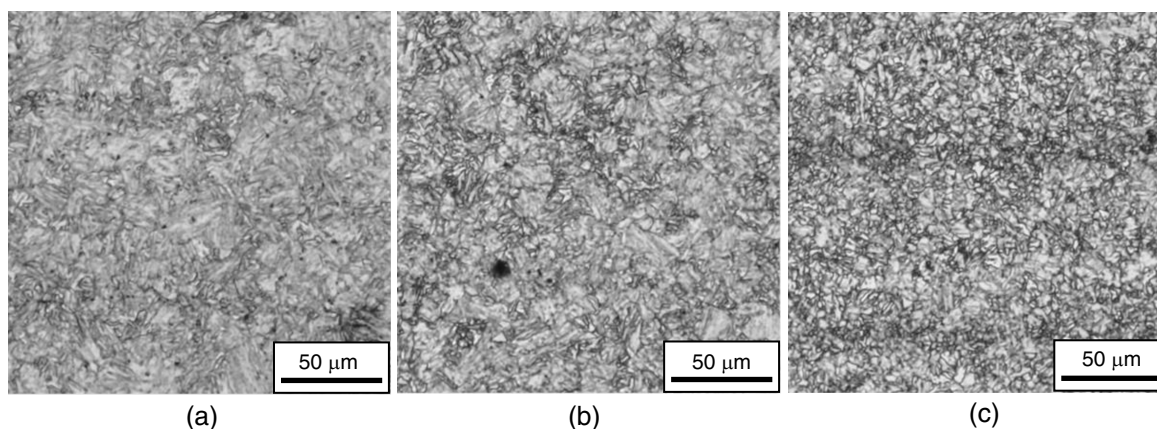


FIGURE 1. Optical image of the microstructure for different high-strength Q&T steels used in the present study (etched by 3% Nital): (a) nonalloyed steel, (b) 1% Cr steel, and (c) 1% Mo steel.

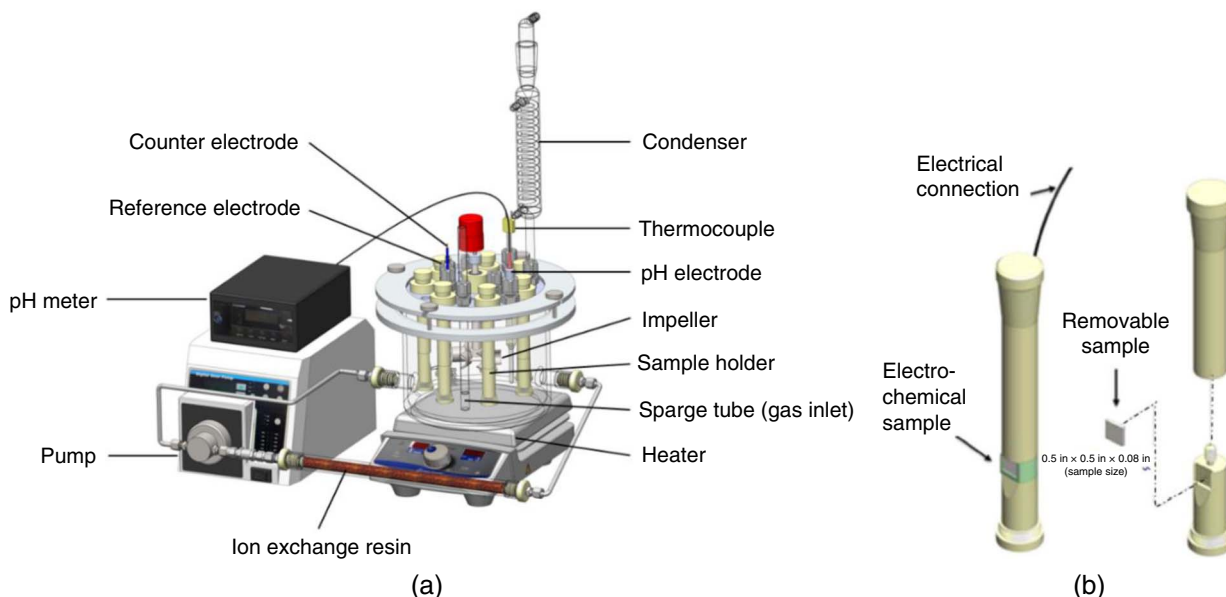


FIGURE 2. Schematic of experimental setup: (a) glass cell equipped with water chemistry control system and (b) removable specimen holders.

the glass cell was equipped with a pump and a flow-through column containing sodium (Na)-form ion-exchange resin. The ion-exchange resin interchange ions by accepting Fe^{2+} from the solution and releasing Na^+ to the solution to maintain a charge balance (more details about this experimental setup are provided elsewhere¹⁴⁻¹⁵).

2.3 | Methodology

Table 2 showed details of experimental conditions in the present study. The pH and temperature were selected to maintain near-saturated conditions with respect to FeCO_3 , where the formation of FeCO_3 is possible but protection is not certain.

An aqueous electrolyte was prepared from deionized water with 1 wt% NaCl. The solution was initially deoxygenated by bubbling CO_2 for at least 2 h prior to insertion of the specimens. This assured that the dissolved oxygen levels were kept below 20 ppb, which was measured by an Orbisphere oxygen

analyzer. The initial pH of the solution was adjusted by adding deoxygenated NaHCO_3 . The solution pH was controlled during the experiment by manually injecting deaerated HCl or NaHCO_3 to maintain the solution pH within $\text{pH } 5.7 \pm 0.15$. The solution temperature was maintained at $80 \pm 1^\circ\text{C}$. After starting the experiment, Fe^{2+} concentration in the solution was measured periodically (once or twice a day) by ultraviolet/visible spectrophotometry. When the measured Fe^{2+} concentration reached or exceeded the target value (~ 15 ppm in this study), the solution was passed through the Na-form ion exchange resin column for 10 min to 20 min with a flow rate of 200 mL/min to 250 mL/min to maintain the target concentration of Fe^{2+} and a stable bulk saturation level (S_{FeCO_3}) of around 1.

The corrosion properties of steels were evaluated by electrochemical techniques (open-circuit potential [OCP] and linear polarization resistance [LPR] measurements). LPR measurements were performed by sweeping the potential from -10 mV to $+10$ mV with respect to the OCP with a scan rate of 0.166 mV/s. The polarization resistance (R_p , Ω) obtained from LPR measurement was used to calculate the corrosion current density (i_{corr} , A/m^2) by using Equation (4):¹⁶

$$i_{\text{corr}} = \frac{B}{S R_p} \quad (4)$$

where S is the specimen surface area (m^2). An empirical B value of 26 mV was used in the present study which is a commonly accepted value in typical CO_2 aqueous environments.¹⁴ Then, the i_{corr} was converted into corrosion rate (CR) using Equation (5):¹⁷

$$\text{CR} = \frac{3.27 \times 10^{-11} \cdot i_{\text{corr}} \cdot \text{EW}}{\rho} \quad (5)$$

where EW is the equivalent weight (kg), ρ is density of iron (kg/m^3), and 3.27×10^{-11} is a constant factor for unit conversion to mm/y.

Parameter	Description
Materials	Nonalloyed steel, 1% Cr steel, and 1% Mo steel
Partial pressure of CO_2	0.53 bar
Temperature	80°C
Test solution	1 wt% NaCl
Initial solution pH	5.7 (adjusted by NaHCO_3)
Solution volume	3.8 L
Stirring solution	Impeller 20 rpm (equivalent to 0.3 m/s in a 0.1 m ID pipe)
Control of Fe^{2+}	Maintain 15 ppm with Na^+ ion exchange resin
Control of solution pH	Manual injection of deaerated HCl or NaHCO_3

After the corrosion experiments, ex situ analyses of the morphology and compositions of corrosion product layers were conducted by using scanning electron microscopy (SEM), energy dispersive x-ray spectroscopy (EDS), x-ray diffraction (XRD), and transmission electron microscopy (TEM) combined with focused ion beam (FIB) milling. Specimen mounted in the epoxy was used for cross-sectional analysis.

RESULTS

3.1 | Corrosion Behavior of Nonalloyed Steel

Figure 3 shows the variations in CR and corrosion potential with time monitored by LPR measurement for nonalloyed steel in 1 wt% NaCl at pH 5.7 and 80°C. The reproducibility of results was shown by the error bars, representing the maximum and minimum values from two different experiments. The CR was about 6 mm/y at the beginning of the experiment and during the first day of exposure, it increased to approximately 10 mm/y accompanied by increasing corrosion potential from -0.7 V to -0.66 V. This is related to the preferential dissolution of ferrite caused by a galvanic coupling with iron carbide (Fe_3C).¹⁸⁻¹⁹ After that, the CR remained relatively stable (10 mm/y to 11 mm/y) for 3 d, as the corrosion potential continued to slowly increase. After 4 d, the CR began to decrease dramatically as the corrosion potential increased further due to the precipitation of FeCO_3 layer. At the end of exposure (approximately one week), the final CR of the nonalloyed steel was around 1 mm/y with a trend of very slow further decrease.

It is noteworthy that the corrosion rates of the nonalloyed steel were higher than those from other work conducted at similar conditions. This could be related to the bulk water chemistry, which was controlled to maintain near-saturated conditions with respect to FeCO_3 in the present study.¹⁴ Figure 4 shows the measured bulk solution pH and Fe^{2+} concentration over the entire testing time. The arrow indicates the time when the solution pH or Fe^{2+} concentration was adjusted, and both values before and after the adjustment are also shown in Figure 4. As shown in Figure 4, the pH of the bulk solution was maintained around the target pH value of 5.7, within 0.1 pH unit. After the first day of experimentation, the concentration of Fe^{2+} was controlled at an average of 15 ppm

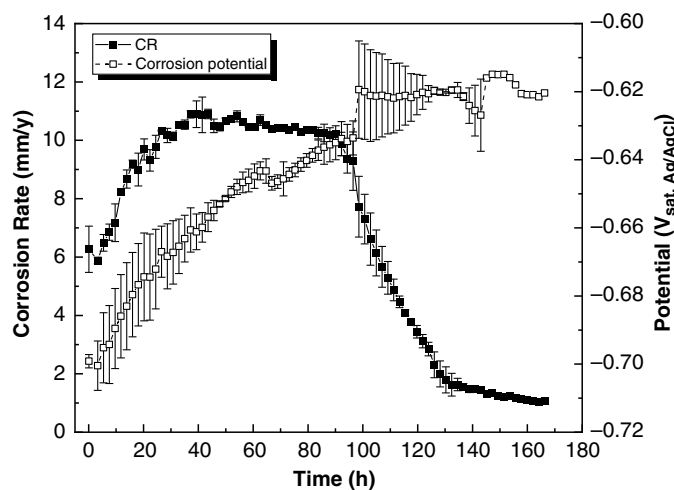


FIGURE 3. Variations of CR and corrosion potential for the nonalloyed steel with time in CO_2 -saturated 1 wt% NaCl solution (pH 5.7 and 80°C).

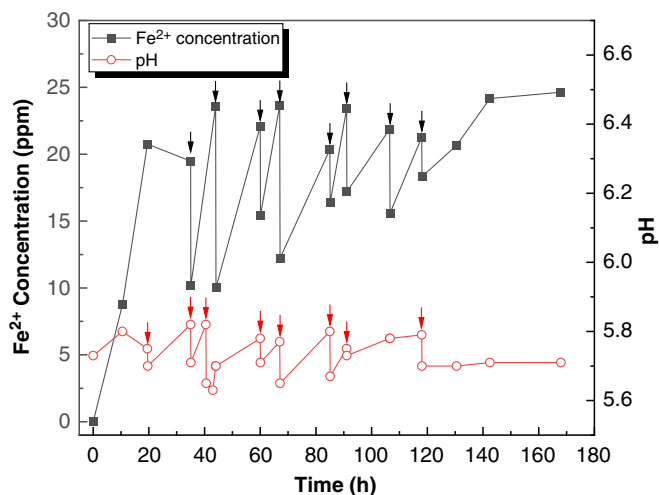


FIGURE 4. Controlled solution pH and Fe^{2+} concentration during the test with nonalloyed steel in CO_2 -saturated 1 wt% NaCl solution at pH 5.7 and 80°C. (The arrows indicate the time when the solution pH or Fe^{2+} concentration was adjusted, and both values before and after the adjustment are shown.)

over the entire length of the experiment, with a slightly increasing trend. If the bulk water chemistry is not controlled, the solution pH and Fe^{2+} concentration would increase with time which could result in lower corrosion rates and faster FeCO_3 formation on the steel surface.

Figure 3 also shows that the CR changed with time although the bulk water chemistry was controlled. To find the reasons for the change in the CR and the surface condition, the specimen was taken out of the solution on days three, five, and seven during the experiment and analyzed for surface morphology and chemical composition. Figure 5 represents the surface and cross-sectional SEM images of the corroded nonalloyed steel after 3 d, 5 d, and 7 d of exposure. After 3 d (72 h), there was a thin and continuous corrosion product layer on the steel surface. TEM analyses shown in Figure 6, reveal that the layer is composed of needle-shaped Fe_3C which is a few hundred nm long. The layer is formed by the emergence of Fe_3C remaining on the metal surface due to the preferential dissolution of ferrite in the early stage of corrosion.¹⁹ The measured corrosion rate after 3 d was approximately 10 mm/y, indicating that the Fe_3C layer is not protective. The surface of the specimens exposed for 5 d (120 h) and 7 d (168 h, end of the test) is very similar to that of the specimen exposed for 3 d, except for the presence of cracks. However, significant differences were found in the cross-sectional observation. It can be seen that a second phase precipitated evenly along the entire steel surface close to the steel surface, and it became denser and grew with time. According to EDS analysis (Figure 7), this inner layer mainly consists of Fe, C, and O, which could be identified as FeCO_3 , whereas the outer layer consists of Fe and C, indicating Fe_3C . The Au seen in the EDS spectra is from the sputter-coated gold used to avoid charging during SEM imaging. A similar “duplex” corrosion product layer structure (Fe_3C as the outer layer and FeCO_3 as the inner layer) has been observed under different experimental conditions in CO_2 environments.^{12,15,20}

Although the Fe_3C layer formed on the nonalloyed steel at the initial stage of exposure was not protective, it restricted the diffusion of corrosion reactants and products through the

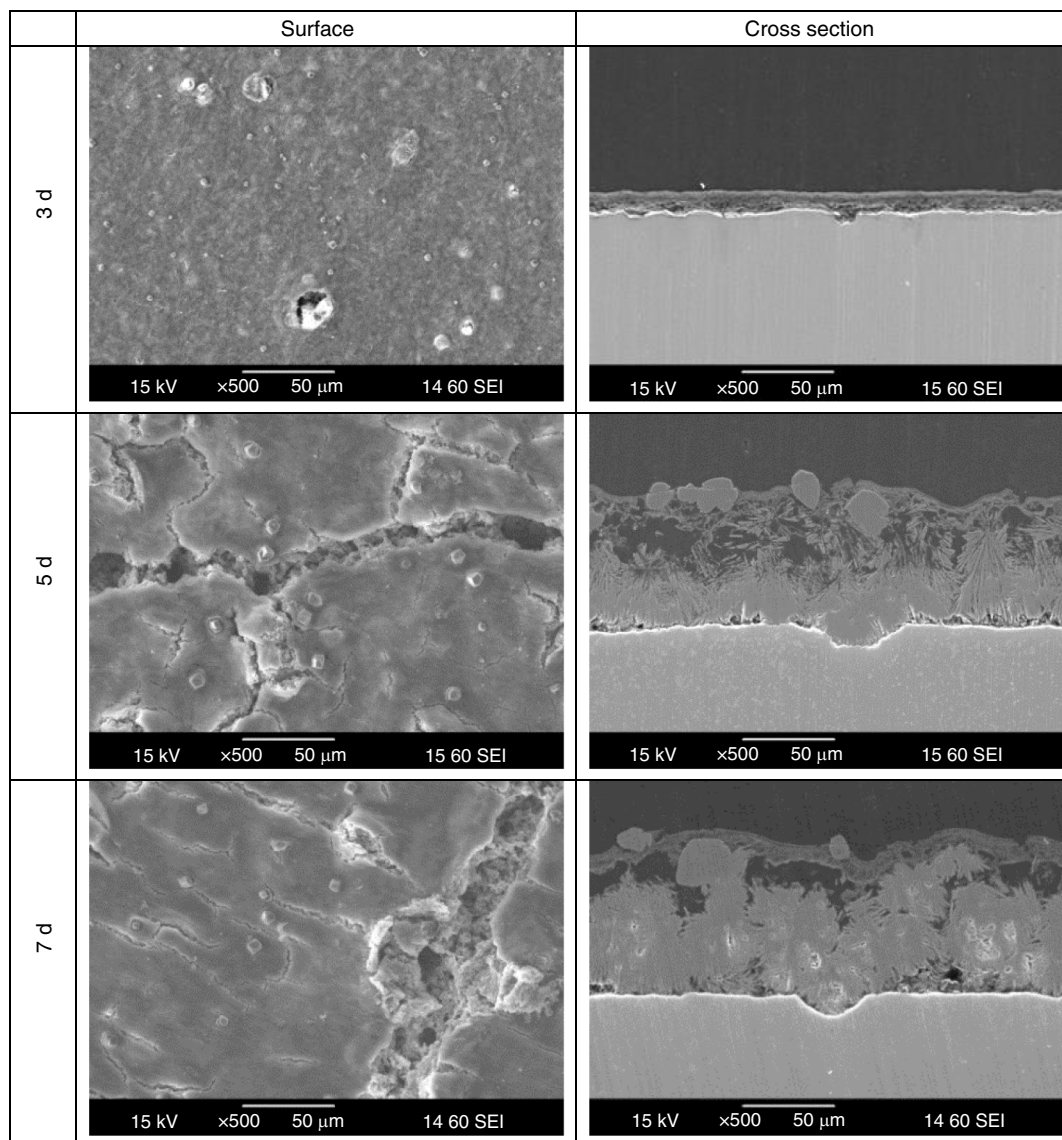


FIGURE 5. SEM surface and cross-section images of the corroded nonalloyed steel exposed to CO_2 -saturated 1 wt% NaCl at pH 5.7 and 80°C .

layer and resulted in an accumulation of Fe^{2+} and a higher pH at the steel surface despite the bulk water chemistry was controlled. Consequently, S_{FeCO_3} near the steel surface within the Fe_3C layer became significantly higher than that of the bulk solution. Such local conditions promoted the precipitation of a FeCO_3 layer at the steel surface, resulting in a decrease in the CR. However, the level of protectiveness by a FeCO_3 layer was relatively low in this case as the final CR was 1 mm/y. Furthermore, the undermining effect at the interface between FeCO_3 and steel is observed (Figure 5). This indicates that only partially protective FeCO_3 layers formed on the surface of nonalloyed steel when the bulk water chemistry was maintained near-saturated condition with respect to FeCO_3 .

3.2 | Corrosion Behavior of 1% Cr Steel

The variations in CR and corrosion potential with time for 1% Cr steel are shown in Figure 8. Unlike the nonalloyed steel, the

CR and corrosion potential did not change as much with time for 1% Cr steel. The CR increased only slightly from 4.5 mm/y to 5.5 mm/y during the first 24 h and then somewhat decreased over the course of the next few days, and then remained stable value in the range of 3 mm/y to 4 mm/y, indicating no formation of FeCO_3 . As shown in Figure 9, the bulk solution pH was maintained at 5.7 and the concentration of Fe^{2+} was controlled at an average of 15 ppm during the experiment.

As in the previous experiment, the specimen was taken out of the solution after 3 d, 5 d, and 7 d to analyze surface morphology and chemical composition. The surface and cross-sectional SEM images of the 1% Cr steel after 3 d, 5 d, and 7 d are shown in Figure 10. The steel surface was covered by a discontinuous “island-shaped” corrosion product layer starting from the 3 d of exposure. Then, at 5 d and 7 d, another somewhat different porous layer is seen underneath the initial layer as shown in the cross-sectional images. According to the EDS analysis shown in Table 3, both inner and outer layers contain Cr, O, and Fe. It should be noted that the presence of C

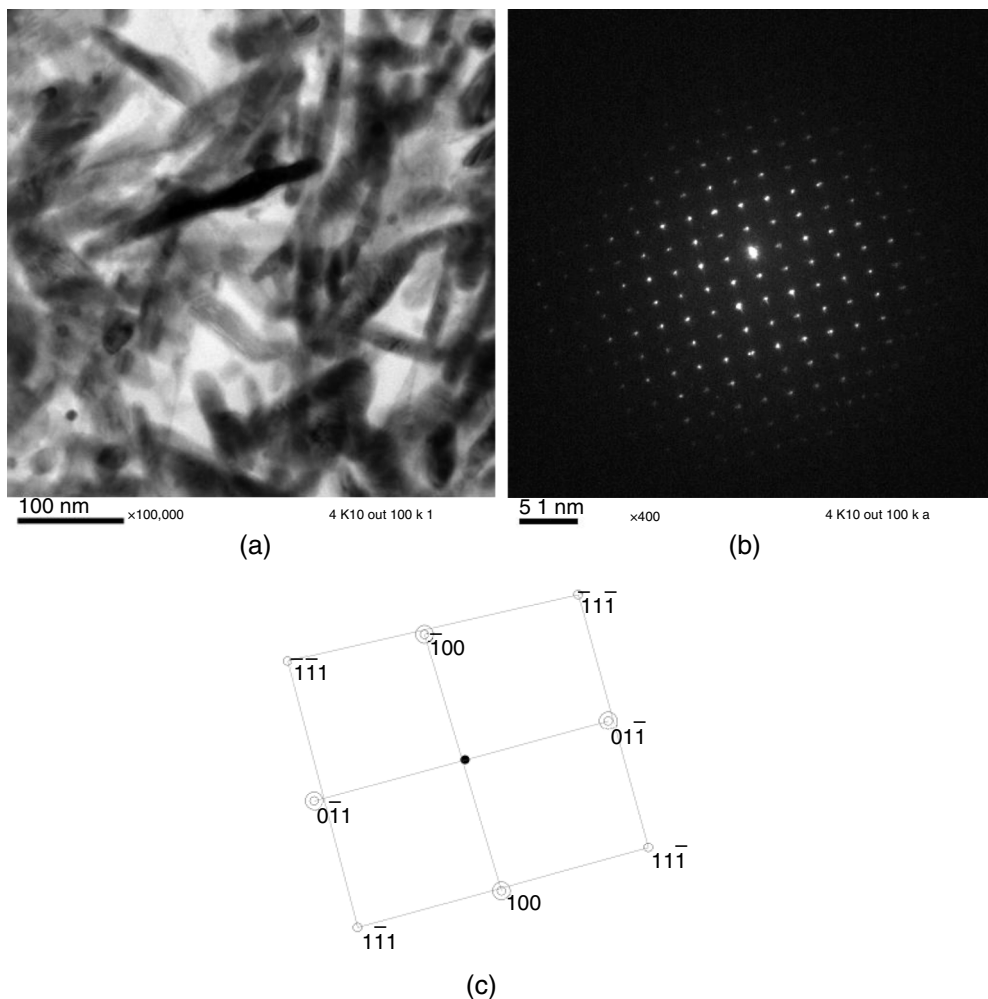


FIGURE 6. Results of TEM analysis for the corrosion product layer on the surface of nonalloyed steel after 3 d of exposure: (a) high-magnification TEM image, (b) electron diffraction pattern for [011] Fe_3C , and (c) Miller indices of [001] Fe_3C .

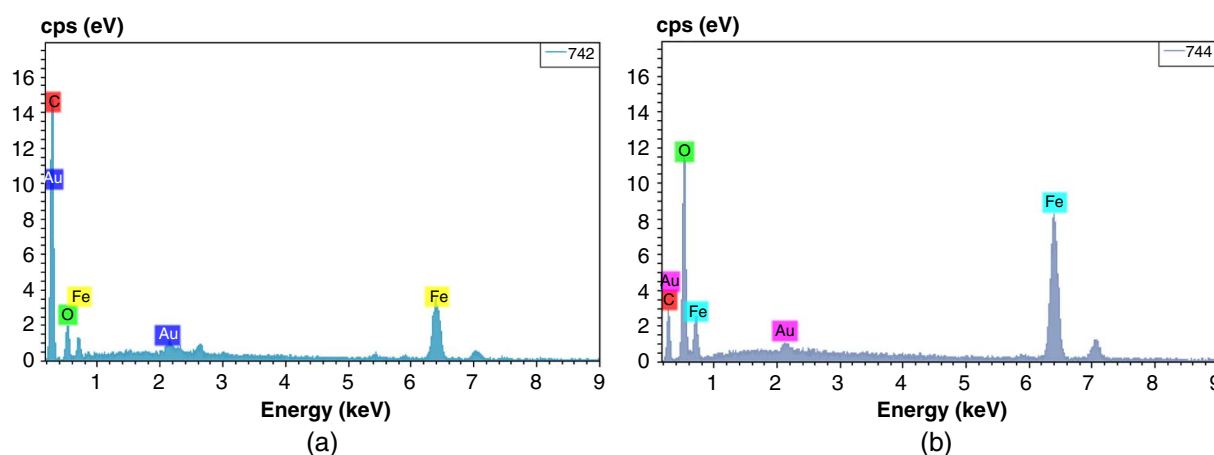


FIGURE 7. EDS spectra of the corrosion product layers on nonalloyed steel after 7 d of exposure: (a) Outer layer and (b) inner layer.

in the corrosion layer here and in every other cross-section EDS analysis is usually not a reliable value, due to the high C content in the epoxy resin used for mounting. The outer layer has relatively higher Cr and O contents compared to the inner layer. In order to identify the corrosion product layers formed on

1% Cr steel, XRD analysis was conducted for the specimen taken after 7 d (Figure 11). Although the thickness of the corrosion product layers observed in the cross-sectional SEM image (Figure 10), was about 30 μm , only the Fe peak for the BCC structure was detected in the XRD analysis. This indicates that

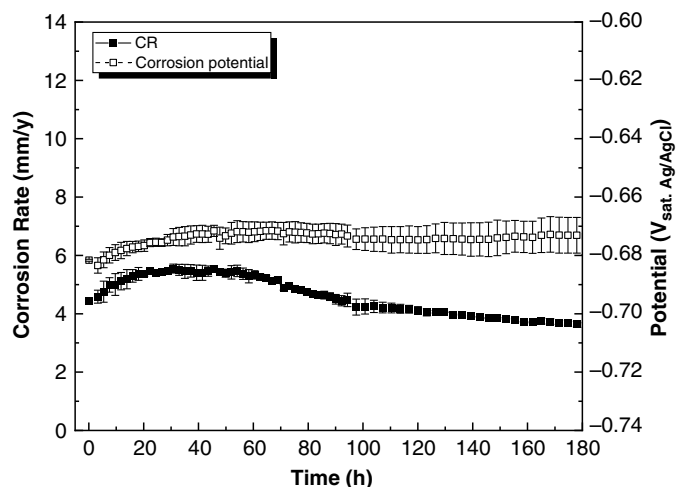


FIGURE 8. Variations of CR and corrosion potential for the 1% Cr steel with time in CO_2 -saturated 1 wt% NaCl solution (pH 5.7 and 80°C).

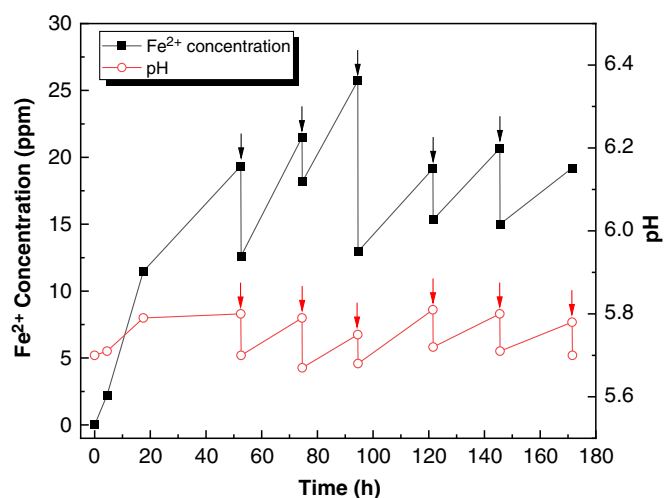


FIGURE 9. Controlled solution pH and Fe^{2+} concentration during the test with 1% Cr steel in CO_2 -saturated 1 wt% NaCl solution at pH 5.7 and 80°C . (The arrows indicate the time when the solution pH or Fe^{2+} concentration was adjusted, and both values before and after the adjustment are shown.)

the corrosion product layers formed on 1% Cr steel could be amorphous or nanocrystalline, and hence were undetectable by XRD analysis.

Further analysis of the outer and inner corrosion product layers was conducted by using TEM. Figure 12 shows the results of TEM analysis for the outer layer formed on the specimen taken after 7 d. It can be seen from the high-magnification image (Figure 12[a]) that the layer is composed of black dots in a gray matrix. The black dots are identified as Fe_3C from the electron diffraction pattern analysis, whereas the matrix (marked as "A" in Figure 12[a]) shows a ring-like diffraction pattern, confirming that it is an amorphous phase (Figure 12[b]). EDS spot analysis from the area "A" indicated that the matrix is mainly composed of Cr and O (Figure 12[c]). Figure 13 shows the results of TEM-EDS mapping analysis for the outer layer. Cr and O are evenly distributed in the layer and Fe is detected where Fe_3C is

present. Figures 14 and 15 demonstrate the results of TEM analysis for the inner layer formed on the specimen taken after 7 d. It shows a similar structure as the outer layer: Cr- and O-containing amorphous matrix with Fe_3C . However, it has more Fe_3C compared to the outer layer.

The results of surface and cross-sectional analysis of 1% Cr steel show that the structure and the chemical composition of the corrosion product layers are completely different from that of nonalloyed steel. The FeCO_3 formed on the nonalloyed steel was not observed at all at the 1% Cr steel exposed at identical conditions, but rather a discontinuous layer containing Cr and O was formed. Although this layer did not offer any real protection, the corrosion rates of 1% Cr steel (4.5 mm/y to 5.5 mm/y) were lower than those of nonalloyed steel (6 mm/y to 11 mm/y) during the first 3 d of the exposure. As mentioned earlier, the galvanic coupling between ferrite and Fe_3C accelerated the corrosion reaction, resulting in high corrosion rates for nonalloyed steel. For the 1% Cr steel, however, it can be speculated that the galvanic effect between ferrite and the Cr-containing corrosion product layers is reduced as the electrical conductivity of corrosion product layers decreases as the content of less-conductive Cr-containing compound increases in the corrosion product layers.²¹ Furthermore, due to the structure of the discontinuous "island-shaped" corrosion product layers, it is hard to create the conditions for Fe^{2+} to accumulate on the steel surface, indicating that S_{FeCO_3} near the steel surface could be similar to that of bulk solution which adversely affects the formation of FeCO_3 .

3.3 | Corrosion Behavior of 1% Mo Steel

Figure 16 shows the variations in CR and corrosion potential with time monitored by LPR measurement for 1% Mo steel. The CR gradually increased from 4.5 mm/y to 8 mm/y during the first few days of exposure and then it decreased and reached around 5.4 mm/y at the end of the exposure. The corrosion potential showed a similar trend with the CR. As this was similar to what was seen on 1% Cr steel, the formation of FeCO_3 was not expected for 1% Mo steel either. Figure 17 shows the measured solution pH and Fe^{2+} concentration over the entire testing time. The pH of the bulk solution was maintained close to 5.7 and the concentration of Fe^{2+} was controlled at an average of 15 ppm over the entire experiment length, just as it was done before.

Figure 18 shows the surface and cross-sectional SEM images of the corroded 1% Mo steel after 3 d, 5 d, and 7 d. The steel surface was covered by a corrosion product layer with cracks that became larger with exposure time. As shown in the cross-sectional SEM images, a porous and nonuniform layer formed on the steel surface after 3 d of exposure. From 3 d to 7 d, the thickness of the layer had not changed but it became denser with time. Furthermore, it showed a rough steel surface underneath the layer due to the corrosion, indicating that this porous layer is not protective. EDS analysis from the specimen taken after 7 d reveals that the layer is mainly composed of Fe, C, O, and Mo (Table 4), and XRD analysis detected Fe_3C and Mo_2C in the corrosion product layer (Figure 19).

Further analysis of the corrosion product layer was conducted by using TEM. Figure 20 shows the results of TEM analysis for the layer formed on the specimen taken after 7 d. The high-magnification image (Figure 20[a]) shows that the layer is composed of black plates and spheroids in a bright gray matrix. The black plates and spheroids are identified as Fe_3C and Mo_2C , respectively from the electron diffraction pattern

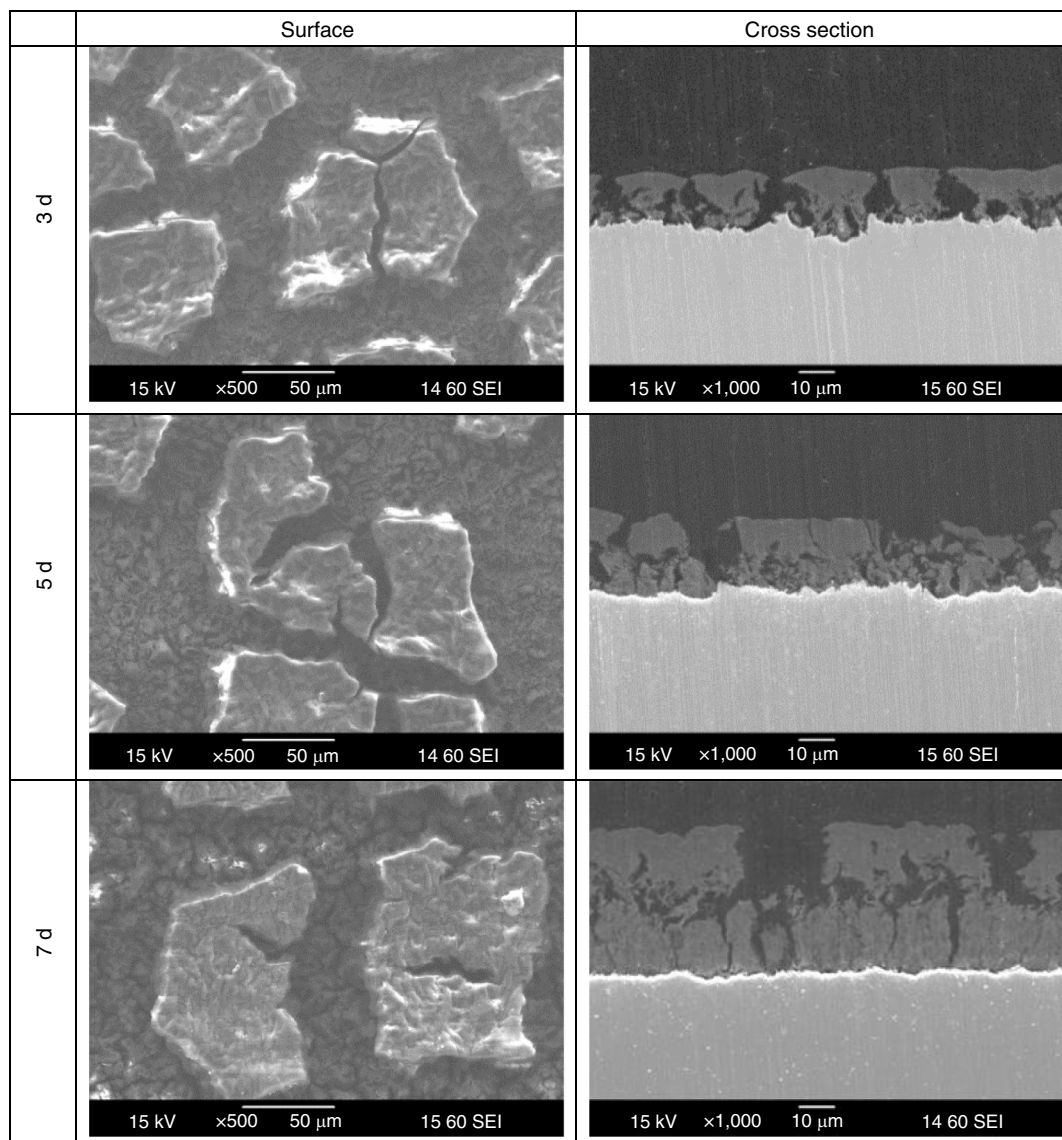


FIGURE 10. SEM surface and cross-section images of the corroded 1% Cr steel exposed to CO_2 -saturated 1 wt% NaCl at pH 5.7 and 80°C .

Table 3. EDS Analysis of 1% Cr Steel Exposed to CO_2 -Saturated 1 wt% NaCl at pH 5.7 and 80°C for 7 d

	Fe (at%)	C (at%)	O (at%)	Cr (at%)
Outer layer	4.2	58.4	20.8	16.6
Inner layer	15.2	64.8	15.9	4.1

analysis, whereas the matrix (marked as "C" in Figure 20[a]) shows a ring-like diffraction pattern, indicating that it is an amorphous phase (Figure 20[b]). EDS spot analysis from the area "C" indicated that the matrix is mainly composed of Mo and O (Figure 20[c]). The results of TEM-EDS mapping analysis (Figure 21) show that Mo and O are distributed in the same places, and they exist in different locations from Fe where Fe_3C presents. The results of TEM analysis suggest that the layer is composed of an amorphous compound containing Mo and O in addition to Fe_3C and Mo_2C .

The starting CR of 1% Mo steel was similar to that of 1% Cr steel (~ 4.5 mm/y), but it increased with time to approximately 8 mm/y, which is a value between 1% Cr steel (~ 5.5 mm/y) and nonalloyed steel (~ 11 mm/y). This indicates that the galvanic effect between ferrite and the corrosion product layers was accelerated for the case of 1% Mo steel due to the different chemical composition of the corrosion product layers compared to the 1% Cr steel. Although it is expected the surface supersaturation to be higher than 1% Cr steel with a higher CR, the formation of FeCO_3 was not observed on the surface of 1% Mo steel. This implies that the discontinuous structure of the corrosion product layers did not act as a diffusion barrier, the same as was observed on the surface of the 1% Cr steel.

DISCUSSION

Figure 22 shows the comparison of the CR with exposure time for the three different steels exposed to the same conditions. All three steels showed a similar trend in the CR with time

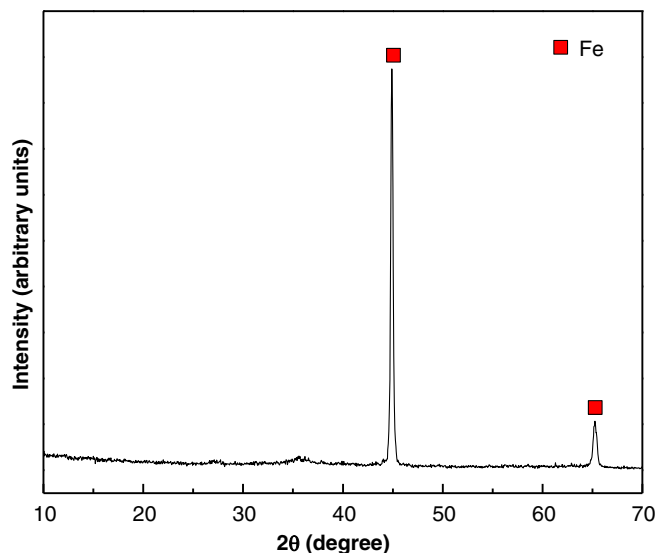


FIGURE 11. XRD patterns of the surface layers formed on 1% Cr steel exposed to CO_2 -saturated 1 wt% NaCl at pH 5.7 and 80°C for 7 d.

(an increase followed by a decrease). However, nonalloyed steel showed the largest initial increase followed by the largest reduction in the CR after 100 h, while the other two steels maintained a high CR to the end of the experiments. Figure 23

shows the changes in bulk saturation value with respect to FeCO_3 for the tests conducted with nonalloyed steel, 1% Cr steel and 1% Mo steel, calculated by Equations (2) and (3). For each measured concentration of Fe^{2+} , the temperature and pH were used to calculate the concentration of CO_3^{2-} from a water chemistry model for CO_2 speciation in aqueous environments.²²⁻²³ As shown in Figure 23, the controlled water chemistry system ensured that the bulk S_{FeCO_3} was slightly above one in all tests independent of steel type.

However, the difference in CR behavior between the nonalloyed steel, 1% Cr steel and 1% Mo steel, is clearly related to the different appearance of the three surfaces. In the case of nonalloyed steel, Fe_3C layer formed early in the experiment, which served as a diffusion barrier (Figures 5 and 6) and became a good matrix for precipitating a semiprotective FeCO_3 layer at the steel surface (Figures 5 and 7). Conversely, a continuous Fe_3C layer did not form in the case of 1% Cr steel and 1% Mo steel. Discontinuous and porous layers with a somewhat different appearance and quite a different composition formed (Figure 10 for 1% Cr steel and Figure 18 for 1% Mo steel), however, this was not followed by the formation of FeCO_3 . This seems odd, as the layers formed on 1% Cr and 1% Mo steels could have also acted as a good matrix for the formation of FeCO_3 , yet this did not happen.

In the case of 1% Cr steel, both the outer and inner corrosion product layers were composed of an amorphous matrix containing Cr and O with Fe_3C dispersed within

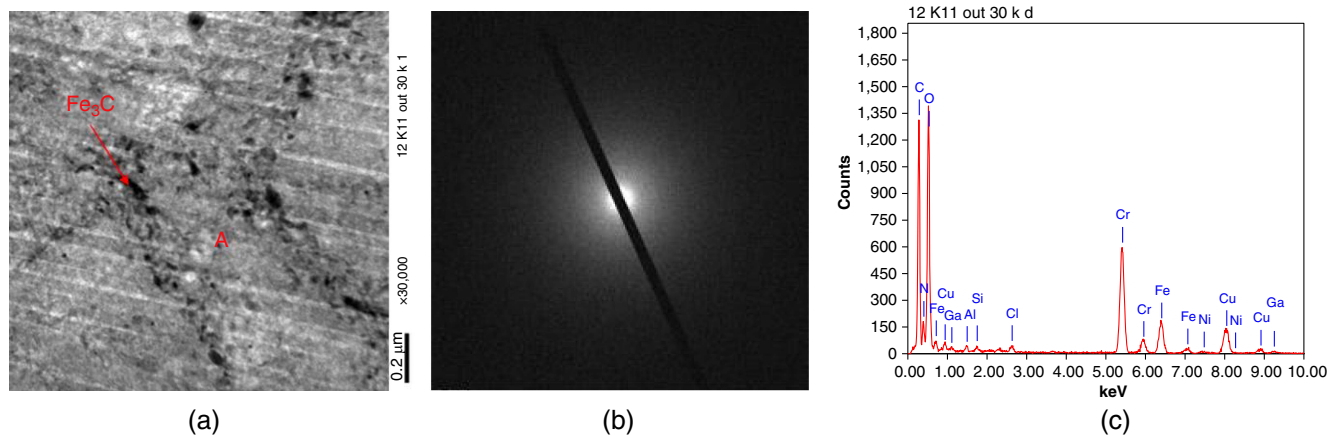


FIGURE 12. Results of TEM analysis for the outer layer on 1% Cr steel surface after 7 d of exposure: (a) high-magnification TEM image, (b) electron diffraction pattern of area "A", and (c) TEM-EDS spectra of area "A".

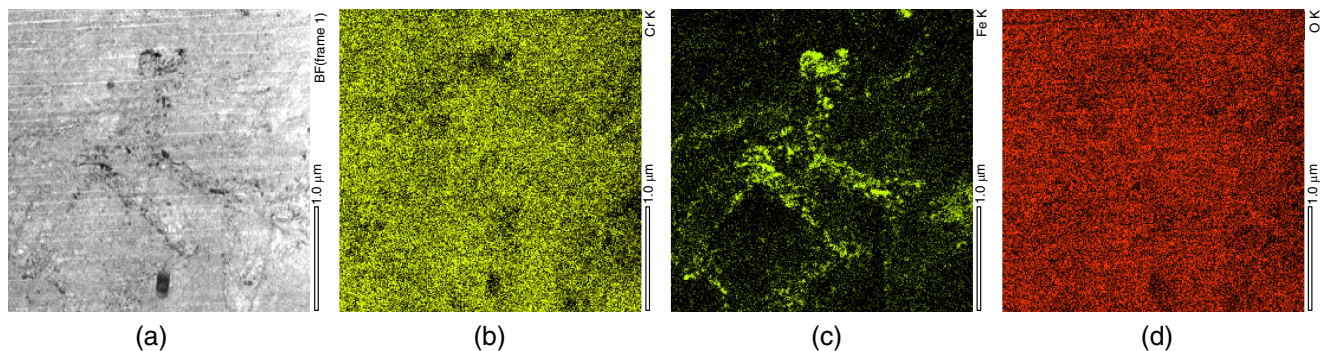


FIGURE 13. Results of TEM-EDS mapping analysis for the outer layer on 1% Cr steel surface after 7 d of exposure: (a) high-magnification TEM image, (b) mapping image for Cr, (c) mapping image for Fe, and (d) mapping image for O.

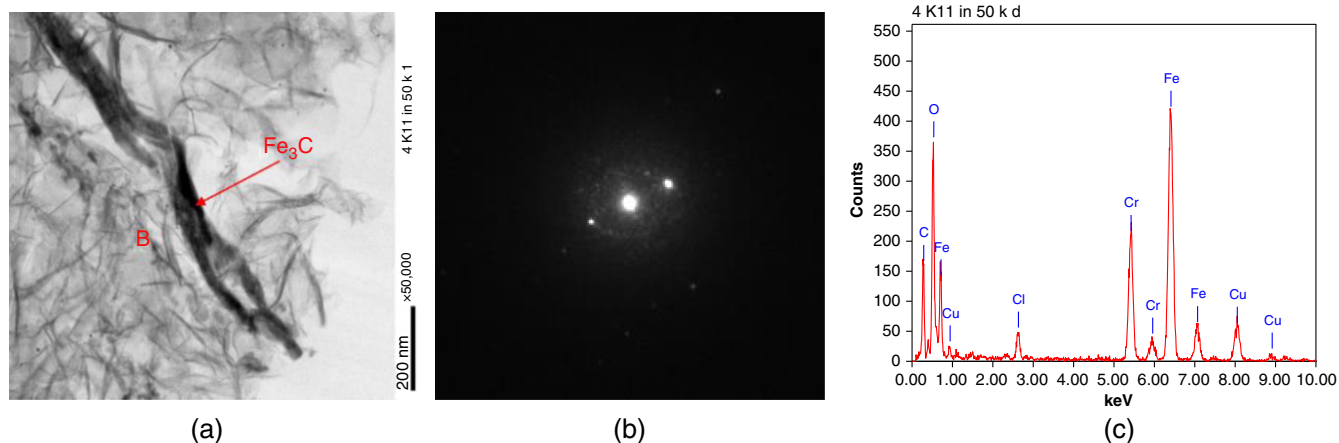


FIGURE 14. Results of TEM analysis for the inner layer on 1% Cr steel surface after 7 d of exposure: (a) high-magnification TEM image, (b) electron diffraction pattern of area "B", and (c) TEM-EDS spectra of area "B".

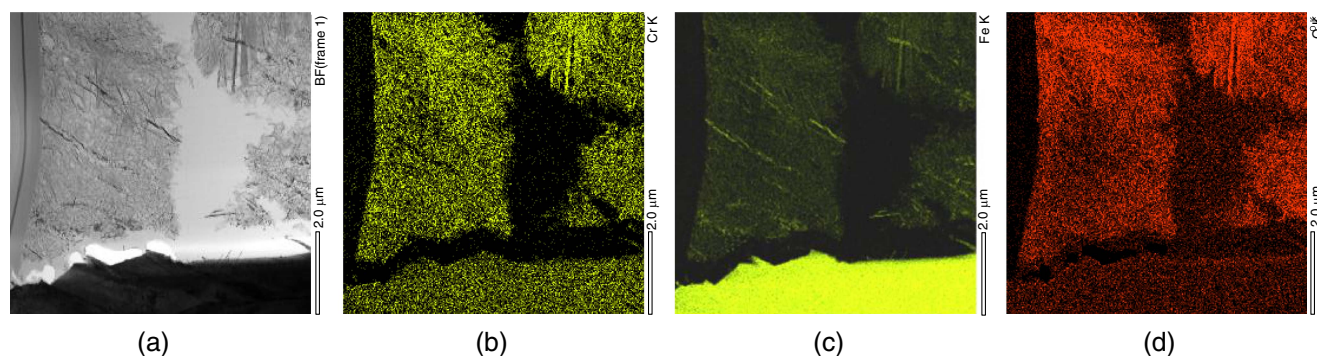


FIGURE 15. Results of TEM-EDS mapping analysis for the inner layer on 1% Cr steel surface after 7 d of exposure: (a) high-magnification TEM image, (b) mapping image for Cr, (c) mapping image for Fe, and (d) mapping image for O.

(Figures 11 through 15). Although it is difficult to identify the exact compound with the analysis methods performed in this study (EDS, XRD, and TEM), based on the surface analysis results and open literature sources, the Cr- and O-containing amorphous material is likely to be chromium(III) hydroxide ($\text{Cr}(\text{OH})_3$).^{7-9,21,24} It has been reported that $\text{Cr}(\text{OH})_3$ formed on a Cr-containing

steel surface can act as a diffusion barrier, similar to Fe_3C , when Cr content is 3% or higher and that it can block corrosive species from reaching the metal surface.^{11,21} However, in the present study, the role of $\text{Cr}(\text{OH})_3$ as a diffusion barrier was not

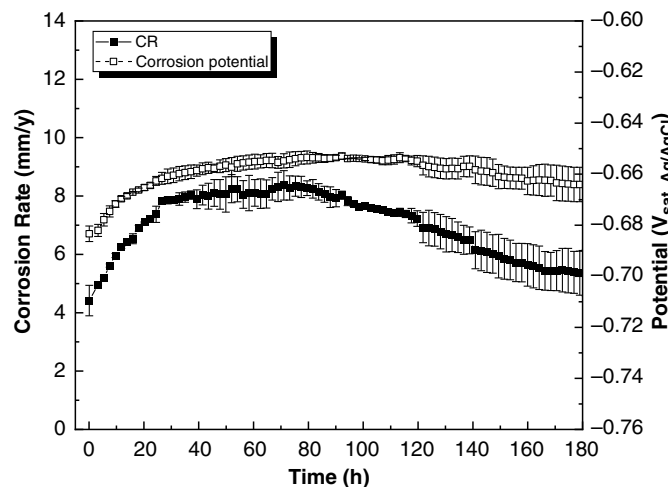


FIGURE 16. Variations of CR and corrosion potential for the 1% Mo steel with time in CO_2 -saturated 1 wt% NaCl solution (pH 5.7 and 80°C).

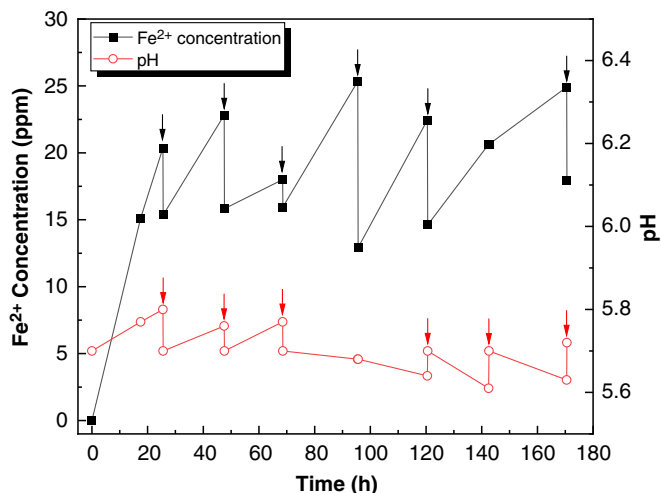


FIGURE 17. Controlled solution pH and Fe^{2+} concentration during the test with 1% Mo steel in CO_2 -saturated 1 wt% NaCl solution at pH 5.7 and 80°C . (The arrows indicate the time when the solution pH or Fe^{2+} concentration was adjusted, and both values before and after the adjustment are shown.)

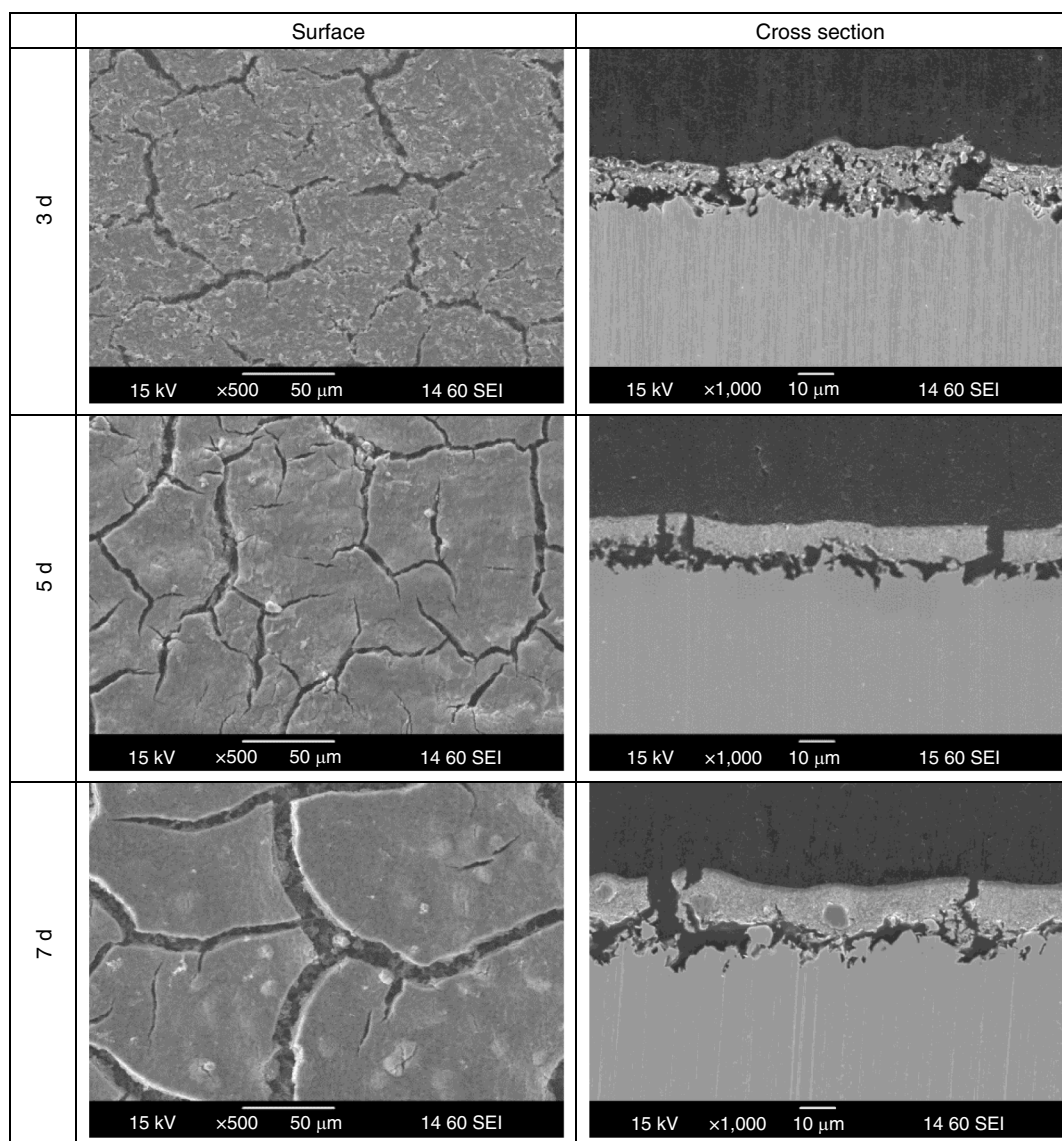
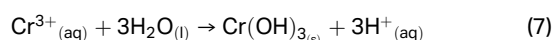


FIGURE 18. SEM surface and cross-section images of the corroded 1% Mo steel exposed to CO_2 -saturated 1 wt% NaCl at pH 5.7 and 80°C .

Table 4. EDS Analysis of 1% Mo Steel Exposed to CO_2 -Saturated 1 wt% NaCl at pH 5.7 and 80°C for 7 d

Fe (at%)	C (at%)	O (at%)	Mo (at%)
41.0	42.4	5.9	9.9

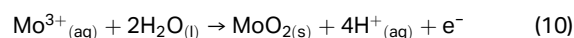
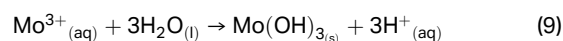
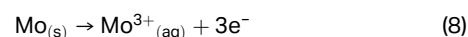
observed for 1% Cr steel, but rather, it somehow made it difficult to form a FeCO_3 , probably by affecting the water chemistry at the steel surface. During corrosion of the 1% Cr steel, Cr can dissolve to give Cr^{3+} and deposit as $\text{Cr}(\text{OH})_3$ which is quite insoluble, via:²⁵



It is important to note that the hydrolysis reaction (Equation [7]) produces H^+ , which can create local acidification at

the steel surface. According to the equilibrium pH expression for the hydrolysis reaction of Cr^{3+} ,²⁶ the equilibrium pH (pH 1.53) is much lower than the bulk solution pH used in the present work (pH 5.7), therefore it is likely that $\text{Cr}(\text{OH})_3$ formed and led to acidification at the surface of 1% Cr steel.

In the case of 1% Mo steel, corrosion behavior similar to that of 1% Cr steel was observed, and the discontinuous corrosion product layers were composed of Mo- and O-containing amorphous matrix with Fe_3C and Mo_2C (Figures 19 through 21). Thus, it is expected that the dissolution of Mo, followed by the hydrolysis reactions of Mo^{3+} happened at the steel surface according to:



It has been reported that both Mo(OH)_3 and MoO_2 are stable when pH is higher than pH 5.²⁷⁻²⁸ The Mo- and O-containing compounds detected by TEM analysis (Figures 20 and 21) can be one of these. According to Reactions (9) and (10), the formation of any of them will

decrease the pH and reduce the S_{FeCO_3} at the surface of 1% Mo steel.

Although the bulk pH was controlled to maintain near saturation conditions for FeCO_3 , the surface pH could be different from the bulk pH, which directly affects the formation

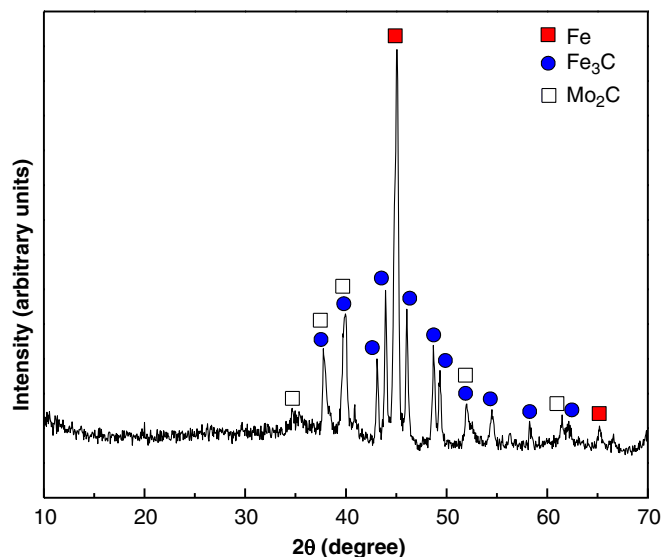


FIGURE 19. XRD patterns of the surface layers formed on 1% Mo steel exposed to CO_2 -saturated 1 wt% NaCl at pH 5.7 and 80°C for 7 d.

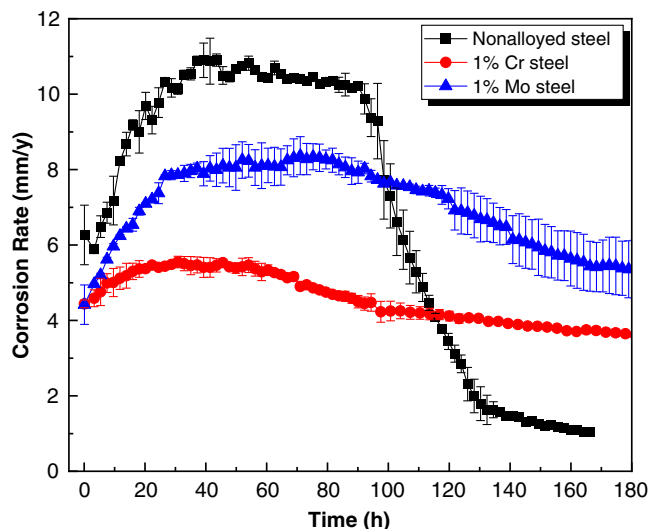


FIGURE 22. Comparison of corrosion rates of different steels exposed to CO_2 -saturated 1 wt% NaCl at pH 5.7 and 80°C.

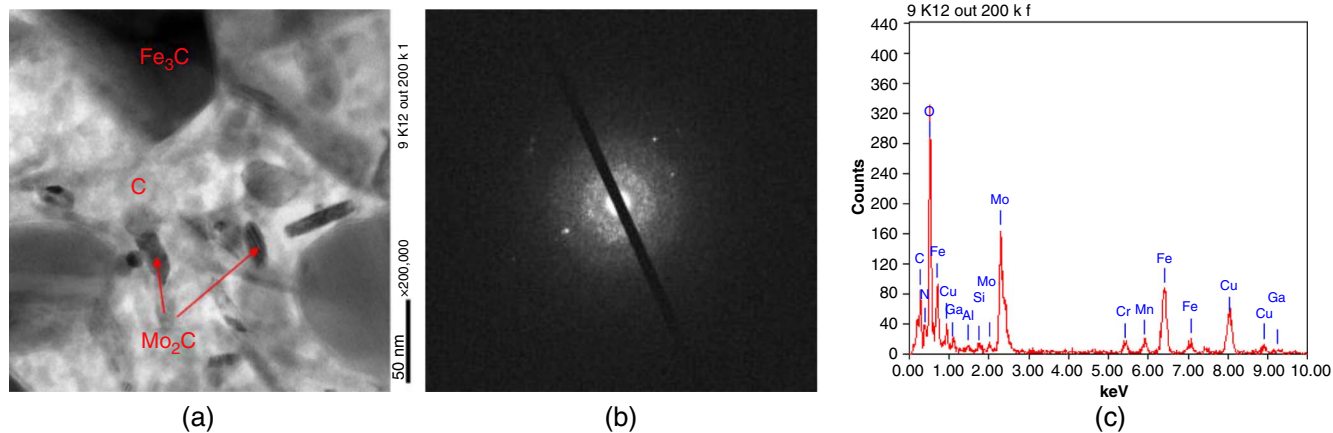


FIGURE 20. Results of TEM analysis for the corrosion product layer on 1% Mo steel surface after 7 d of exposure: (a) high-magnification TEM image, (b) electron diffraction pattern of area "C", and (c) TEM-EDS spectra of area "C".

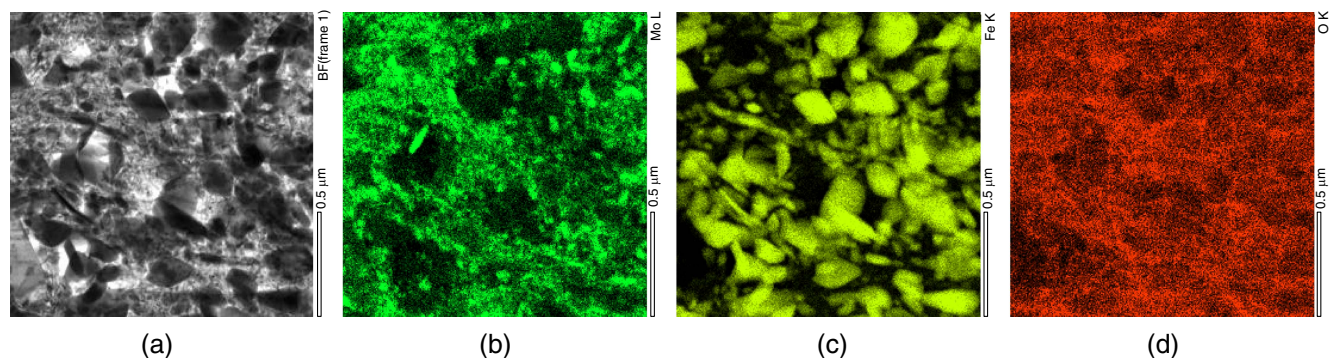


FIGURE 21. Results of TEM-EDS mapping analysis for the corrosion product layer on 1% Mo steel surface after 7 d of exposure: (a) high-magnification TEM image, (b) mapping image for Mo, (c) mapping image for Fe, and (d) mapping image for O.

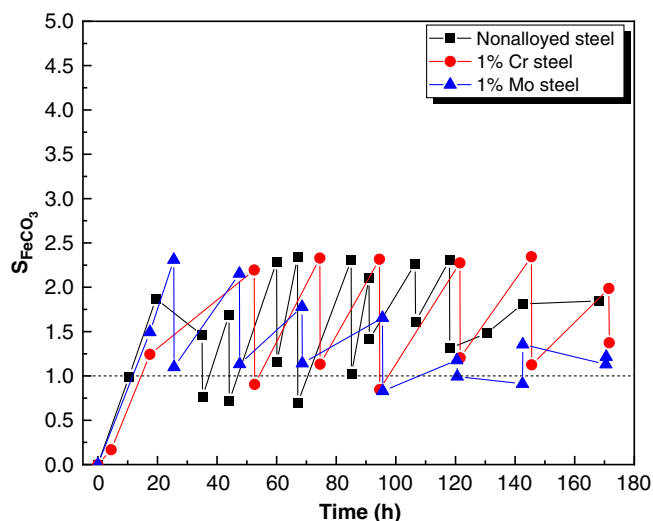


FIGURE 23. Variations of S_{FeCO_3} with time for tests conducted on three different steels in CO_2 -saturated 1 wt% NaCl at pH 5.7 and 80°C.

of $FeCO_3$. Experimental evidence has shown that the pH measured near the surface of corroding steel is 0.5 to 1 pH unit higher than the bulk solution pH of 6.²⁹⁻³⁰ The S_{FeCO_3} was calculated at different pH values assuming that the increase in pH at the surface is similar to that of bulk pH 6 reported in the literature, and the results are plotted in Figure 24 as a function of Fe^{2+} concentration. This indicates that $FeCO_3$ can form even a small amount of Fe^{2+} is present on the surface in the expected surface pH range of 6.2 to 6.7. This could be the case for the nonalloyed steel. For the cases of 1% Cr and 1% Mo steels, however, the surface pH should be lower than the expected surface pH as $FeCO_3$ was not observed on the surface of those steels. This proves that the hydrolysis reactions described above (Equations [7], [9], and [10]) prevented the surface pH from increasing when the bulk chemistry is controlled. And it did not allow the surface S_{FeCO_3} to become high enough to form $FeCO_3$ for 1% Cr and 1% Mo steels.

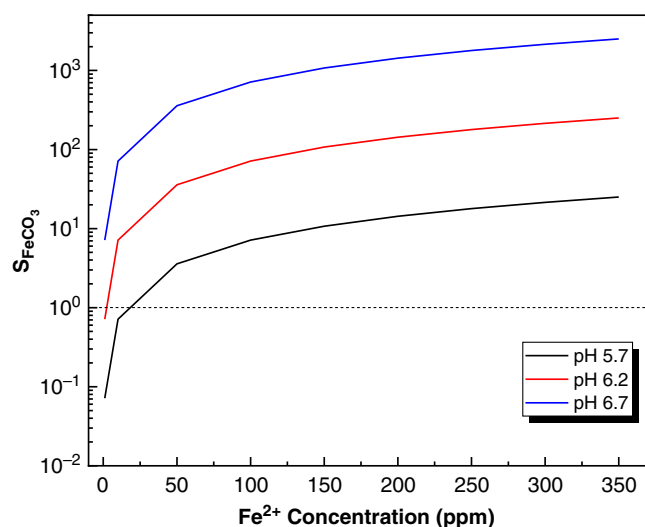


FIGURE 24. Calculated S_{FeCO_3} at 80°C for different pH values as a function of Fe^{2+} concentration.

CONCLUSIONS

The individual effect of a small amount (1 wt%) of Cr and Mo on the formation of $FeCO_3$ was investigated under controlled water chemistry conditions where the bulk S_{FeCO_3} was maintained at near-saturated conditions. The following conclusions are drawn:

- The formation of the Fe_3C layer at the surface of nonalloyed steel created favorable conditions for semiprotective $FeCO_3$ to form, which was otherwise not favored based on the controlled bulk water chemistry.
- $FeCO_3$ was not observed on the surface of 1% Cr steel and 1% Mo steel, but rather discontinuous and porous corrosion product layers were formed, and the CR remained approximately 4 mm/y for 1% Cr steel and approximately 5 mm/y for 1% Mo steel under the experimental conditions of this study.
- The corrosion product layer formed on 1% Cr steel was composed of amorphous $Cr(OH)_3$ with dispersed particles of Fe_3C . A similar structure was observed for 1% Mo steel, which was composed of amorphous $Mo(OH)_3$ and/or MoO_2 with Fe_3C and Mo_2C .
- Due to the hydrolysis reactions of dissolved Cr^{3+} and Mo^{3+} , and the discontinuous structure of the corrosion product layers, the surface conditions for 1% Cr steel and 1% Mo steel were not favorable for the formation of $FeCO_3$ under the experimental conditions of this study.

ACKNOWLEDGMENTS

The authors acknowledge the support of Mr. T. Ohe, Mr. Y. Arai, Mr. J. Nakamura, Mr. H. Kamitani, and Dr. H. Amaya at NIPPON STEEL CORPORATION.

References

1. S. Nešić, *Corros. Sci.* 49, 12 (2007): p. 4308-4338.
2. Z. Ma, Y. Yang, B. Brown, S. Nešić, M. Singer, *Corros. Sci.* 141, 8 (2018): p. 195-202.
3. W. Sun, S. Nešić, R.C. Woollam, *Corros. Sci.* 51, 6 (2009): p. 1273-1276.
4. M.B. Kermani, A. Morshed, *Corrosion* 59, 8 (2003): p. 659-683.
5. L. Wei, X. Pang, K. Gao, *Corros. Sci.* 111, 10 (2016): p. 637-648.
6. M. Ueda, *Corrosion* 62, 10 (2006): p. 856-867.
7. T. Doi, T. Adachi, T. Kubo, N. Usuki, *Corros. Sci.* 177, 12 (2020): p. 108931.
8. Q. Wu, Z. Zhang, X. Dong, J. Yang, *Corros. Sci.* 75, 10 (2013): p. 400-408.
9. S. Guo, L. Xu, L. Zhang, W. Chang, M. Lu, *Corros. Sci.* 63, 10 (2012): p. 246-258.
10. B. Ingham, M. Ko, N. Laycock, N.M. Kirby, D.E. Williams, *Faraday Discuss.* 180, 1 (2015): p. 171-190.
11. W. Li, L. Xu, L. Qiao, J. Li, *Appl. Surf. Sci.* 425, 12 (2017): p. 32-45.
12. Y.S. Choi, S. Nešić, H.G. Jung, *Corrosion* 74, 5 (2018): p. 566-576.
13. M. Hassan Sk, A.M. Abdullah, J. Qi, M. Ko, B. Ingham, N. Laycock, M. P. Ryan, D.E. Williams, *J. Electrochem. Soc.* 165, 5 (2018): p. C278-C288.
14. S. Ieamsupapong, "Mechanisms of Iron Carbonate Formation on Mild Steel in Controlled Water Chemistry Conditions" (Ph.D. thesis diss., Ohio University, 2016).
15. H. Mansoori, D. Young, B. Brown, S. Nešić, M. Singer, *Corros. Sci.* 158, 9 (2019): p. 108078.
16. M. Stern, A.L. Geary, *J. Electrochem. Soc.* 104 (1957): p. 56-63.
17. S.W. Dean, *Handbook on Corrosion Testing and Evaluation* (New York, NY: John Wiley, 1971), p. 171.
18. N. Staicopolus, *J. Electrochem. Soc.* 110, 11 (1963): p. 1121.
19. J. Crolet, N. Thevenot, S. Nešić, *Corrosion* 54, 3 (1998): p. 194-203.
20. W. Li, B. Brown, D. Young, S. Nešić, *Corrosion* 70, 3 (2014): p. 294-302.

21. C.F. Chen, M.X. Lu, Z.H. Zhang, W. Chang, *Corrosion* 61, 6 (2005): p. 594-601.
22. M. Nordsveen, S. Nešić, R. Nyborg, A. Stangeland, *Corrosion* 59, 5 (2003): p. 443-456.
23. S. Nešić, A. Kahyarian, Y.S. Choi, *Corrosion* 75, 3 (2019): p. 274-291.
24. S. Hassani, T.N. Vu, N.R. Rosli, S.N. Esmaeely, Y.S. Choi, D. Young, S. Nešić, *Int. J. Greenhouse Gas Control* 23, 4 (2014): p. 30-43.
25. W. Liu, S.L. Lu, Y. Zhang, Z.C. Fang, X.M. Wang, M.X. Lu, *Mater. Corros.* 66, 11 (2015): p. 1232-1244.
26. T. Suzuki, M. Yamabe, Y. Kitamura, *Corrosion* 29, 1 (1973): p. 18-22.
27. P. Wang, L.L. Wilson, D.J. Wesolowski, J. Rosenqvist, A. Anderko, *Corros. Sci.* 52, 5 (2010): p. 1625-1634.
28. J.B. Lee, *Corrosion* 37, 8 (1981): p. 467-480.
29. J.B. Han, B. Brown, D. Young, S. Nešić, *J. Appl. Electrochem.* 40, 3 (2010): p. 683-690.
30. R. De Motte, R. Mingant, J. Kittel, F. Ropital, P. Combrade, S. Necib, V. Deydier, D. Crusset, *Electrochim. Acta* 290 (2018): p. 605-615.